Langmuir

Letter

pubs.acs.org/Langmuir

Reliable Measurement of the Receding Contact Angle

Juuso T. Korhonen, Tommi Huhtamäki, Olli Ikkala, and Robin H. A. Ras*

Molecular Materials, Department of Applied Physics, Aalto University School of Science (former Helsinki University of Technology), Espoo, Finland

Supporting Information

ABSTRACT: Surface wettability is usually evaluated by the contact angle between the perimeter of a water drop and the surface. However, this single measurement is not enough for proper characterization, and the so-called advancing and receding contact angles also need to be measured. Measuring the receding contact angle can be challenging, especially for extremely hydrophobic surfaces. We demonstrate a reliable procedure by using the common needle-in-the-sessile-drop method. Generally, the contact line movement needs to be followed, and true receding movement has to be distinguished from "pseudo-movement" occurring before the receding angle is reached. Depending on the contact angle hysteresis, the initial size of the drop may need to be surprisingly large to achieve a reliable result. Although our motivation for this work was the characterization of superhydrophobic surfaces, we also show that this method works universally ranging from hydrophilic to superhydrophobic surfaces.

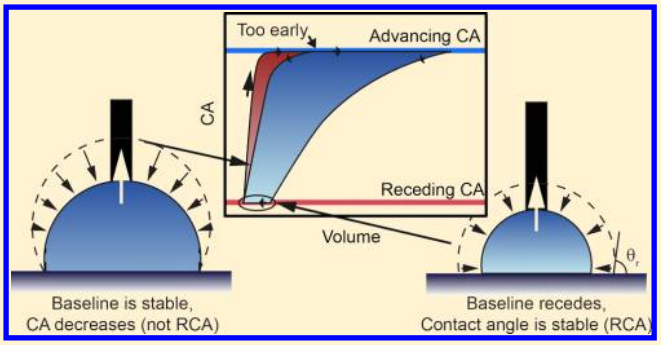

INTRODUCTION

It has been known for a long time that the leaves of the lotus plant repel water to keep themselves clean, an effect now known as superhydrophobicity.[1,2] This refers to a surface that repels water almost perfectly and causes sessile drops to assume a near-spherical shape together with a low roll-off angle.[3] Two surface wetting states are connected to superhydrophobicity: a roughness-induced fully wetting *Wenzel* state[4] and a composite wetting *Cassie–Baxter* state,[5] where an air cushion is trapped below the roughness features. The term "superhydrophobic" has been around for at least four decades,[6] yet it still has not been unambiguously defined. Most commonly, superhydrophobic surfaces are defined by having an apparent contact angle (CA, θ) higher than 150° with a roll-off angle (i.e., sliding/slip angle) less than 10°.[9] However, this definition is found incomplete in two ways. First, it does not tell which CA should be measured (probably the *most stable contact angle* (MSCA, θ_{ms}), which is thermodynamically the most stable CA). Second, the roll-off angle depends on the drop size and the type of surface roughness.[10,11] We interpret superhydrophobicity such that the *lowest* measurable (static) CA, i.e., the *receding contact angle* (RCA, θ_r) is higher than 150°. Correspondingly, the highest measurable CA is called the *advancing contact angle* (ACA, θ_a). This interpretation ensures that the second requirement for a low roll-off angle is automatically met for drops larger than ca. 10 μL, as it lowers the amount of work for adhesion,[11] $W \sim \cos\theta_r - \cos\theta_a$.

Both the ACA and the RCA are *(quasi-)static* contact angles, i.e., the speed of the moving contact line is kept so slow that it does not affect the CA and thus any dynamic effects are suppressed.[12,13] The difference of the ACA and the RCA, $\Delta\theta = \theta_a - \theta_r$, is called *contact angle hysteresis*. However, this hysteresis value reflects no physical quantity. In addition, $\cos\theta_r - \cos\theta_a$ has been used to describe hysteresis,[14] yet its value is difficult to comprehend, as it ranges from −2 to 0. Hence, we propose to define a "hysteresis percentage" value as $\Delta\theta_{\%} = (\cos\theta_r - \cos\theta_a)/2 \times 100\%$, which ranges from 0%, for no hysteresis, to 100%, for maximum hysteresis. It is linearly proportional to the work of adhesion, $W \sim \Delta\theta_{\%}$, so the hysteresis values can be directly compared with each other to see how movement is facilitated on a specific surface—unlike with $\Delta\theta$. No simple universal equation exists to extract the MSCA from the ACA and the RCA,[13] although previously the MSCA was found to approximately follow $\cos\theta_{ms} = (\cos\theta_a + \cos\theta_r)/2$.[14,15] This approximation together with the hysteresis percentage leads to $\cos\theta_a = \cos\theta_{ms} - \Delta\theta_{\%}$ and $\cos\theta_r = \cos\theta_{ms} + \Delta\theta_{\%}$. Furthermore, it is always necessary to report *both* the ACA and the RCA and also to describe what kind of measurement was used, as the tilting plate experiments tend to yield different results compared to the needle-in-the-sessile-drop method.[11,16]

The most common method for measuring contact angles is probably the *sessile drop method*, also known as the *goniometer method*, i.e., a drop of liquid is suspended on a surface and the CA is measured either using a goniometer or a (semi)automatic computer image recognition technique. In computerized analysis, the points of contact (the triple line) are first identified. This is a highly delicate process where small variations can lead to large errors in the measured CA—

Received: January 2, 2013
Revised: February 28, 2013
Published: March 1, 2013

   dx.doi.org/10.1021/la400009m | *Langmuir* 2013, 29, 3858–3863

especially for high CA surfaces.[17−19] Then, the perimeter of the drop is analyzed and a theoretically calculated shape of a drop is fitted into the data. The theoretical shape can be a sphere or an ellipse, yet most typically a Young−Laplace fit based on axisymmetric drop shape analysis[20] is done for high CA surfaces. It has also been pointed out that small variations in the focus and lighting conditions can lead to variations of several degrees in the measured CA.[17]

Using the sessile drop method, the ACA and the RCA can, in principle, be easily measured. To measure the ACA, a needle is used to deposit a small drop (e.g., 1 μL) on the surface while leaving the needle inside the drop (Figure 1a). More liquid is then *slowly* pumped into the drop, which causes the drop to grow. At first, the CA increases (Figure 1b) until suddenly it saturates to a certain value (Figure 1c). This happens at the moment when the contact line starts to advance, i.e., the CA reaches the largest possible value the surface can uphold. This value is the ACA and it can usually be measured with precision and repeatability. To measure the RCA, the opposite should be done: slowly pump liquid out from a sessile drop (Figure 1d,e). Unfortunately, RCA measurements on high CA surfaces turn out to be difficult. Often the measured RCA can seem to be a monotonic function of the drop size. We noticed that this may be due to the contact line not properly receding even though small changes could be observed.

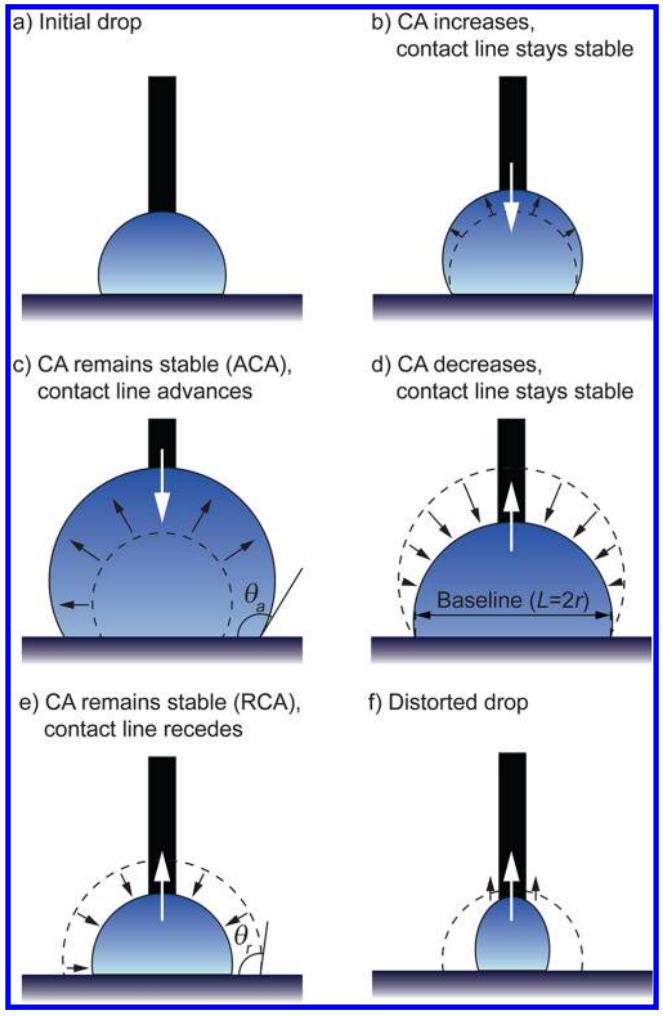

Figure 1. Illustration of a model CA measurement. (a) Small drop is deposited on a surface. (b) Liquid is pumped into the drop and volume increases while the contact line is not advancing. (c) ACA is reached and the contact line starts to advance. The volume is still increased. (d) Liquid is pumped out of the drop and volume decreases, while the baseline does not recede. The CA decreases, because the RCA has not been reached. (e) The RCA is reached and the drop baseline recedes. The CA does not change during this phase. (f) The drop size reaches the same magnitude as the size of the needle and/or the size of the roughness features on the surface. The drop shape is strongly distorted and often the CA decreases or increases rapidly.

We report a reliable procedure to measure the RCA using the needle-in-the-sessile-drop method with commercially available equipment and quantify how large size of droplets should be used for the measurements when the hysteresis is either known or can at least be estimated. The control of the initial drop volume in the RCA measurements is an especially important factor when the surface is "adhesive", which implies that there is large contact angle hysteresis, and thus large drops should be used.

EXPERIMENTAL SECTION

An Attension Theta optical tensiometer with automated liquid pumping system was used for the contact angle measurements. Purified (Milli-Q) and degassed water was used as the probe liquid. Experimental conditions are described in detail in the Supporting Information.

We selected six surfaces for the experiments. Surface (1) was a Si wafer with a nanorough silicone layer. It exhibited a high ACA and remarkably large hysteresis and was thus quantified as an "adhesive hydrophobic" surface. Surface (2) was a Si wafer with silicone nanofilaments[21−24] grown on the surface. It had a high ACA and moderate hysteresis. Surface (3) was similar to (2), but the surface was further passivated with a perfluorinated silane. This superhydrophobic sample had a high ACA and extremely low hysteresis. Surface (4) was a silicon wafer treated with a commercial superhydrophobic coating (Glaco Mirror Coat "Zero"), which created a fractal surface of hydrophobized silica nanoparticles. The ACA for this surface was high with low hysteresis. Surface (5) was a standard polystyrene Petri dish. Surface (6) was a Si wafer without any treatment. Contact angle measurement data are visualized in Figure 2. Details of the measurements, tabulated contact angle data, and further characterization can be found in the Supporting Information.

RESULTS AND DISCUSSION

Contact angle measurement data from surface (1) are shown as a demonstration. This sample was chosen as it demonstrated the volume-dependent behavior most clearly, although the results were generalizable to diverse other surfaces as shown later. To measure the ACA, liquid was pumped into a sessile

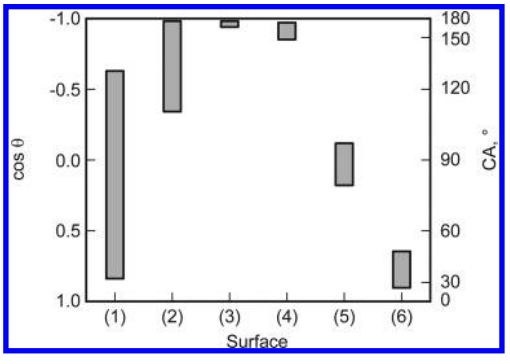

Figure 2. Contact angles and hysteresis range visualized for the surfaces. The hysteresis percentage, $\Delta\theta_{\%}$, which visualizes the work of adhesion, is the length of the bar with 100% being from 0° to 180°.

dx.doi.org/10.1021/la400009m | *Langmuir* 2013, 29, 3858−3863

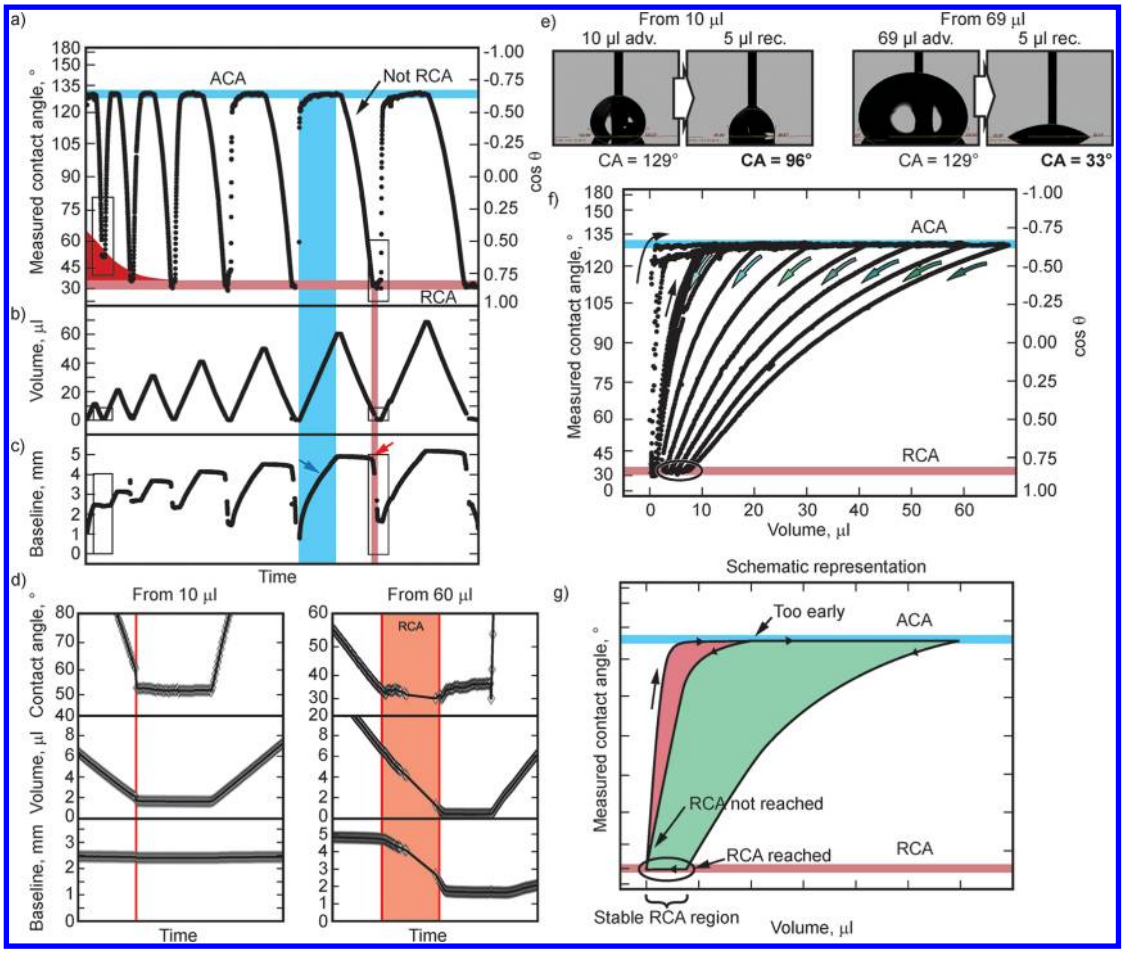

Figure 3. Contact angle measurement of surface (1), which is a high contact angle surface with extremely high hysteresis. Part of the data for drop sizes less than *ca.* 2 μL has been removed, because it could not be fitted with the algorithm used by the software. (a–c) The Young–Laplace fitted CA (the mean from both sides of the drop) as a function of time along with drop volume (determined from fit) and baseline length. The shadowed areas show the ACA measured when the baseline is advancing (blue) and the RCA measured when it is receding (red). The red and blue arrows indicate examples of where the baseline advances or recedes. The black arrow shows an example of a region where the RCA should not be determined, because the baseline is not properly receding. (d) Magnified regions from a to c for the initial drop volumes of 10 μL (left) and 60 μL (right). Magnified locations are marked in a–c with rectangles. The RCA is not reached in the left figure, but is clearly visible in the right. (e) Photos from different phases of the CA measurement for ACA drop volumes of 10 μL (left) and 69 μL (right). There is a clear difference between the photos of the receding drops, while the advancing drops show the same CAs. (f) The CA plotted as a function of drop volume. The arrows indicate measurements to different maximum volumes. (g) shows schematically how the measured CA cannot recede to the RCA if the initial volume is too small.

drop and the CA was simultaneously recorded at roughly 3–10 fps. These data are plotted both as a function of time (Figure 3a) and as a function of volume (Figure 3f). In the plots there are 7 subsequent ACA measurements, where each time the final volume is increased (Figure 3b). The CA saturated quickly to the ACA in each case. This was due to the initial volume of the drop being small—on the order of 2 μL—and thus, the ACA was reached at a relatively small volume, which was in this case less than 10 μL. This could be seen more clearly in the θ/V plot (Figure 3f), where the paths leading to the ACA (marked with black arrows) saturated early depending on the initial drop volume. Using this method, the ACA could usually be reliably measured without problems and the measurements were often possible even for surfaces exhibiting "stick and slip" behavior.

Measuring the RCA was done by decreasing the volume of a sessile drop. In this case, the θ/t plot (Figure 3a) showed that for initial volumes less than *ca.* 30 μL the measured "RCA" reached a value that was dependent on the initial volume. For sufficiently high volume, the lowest measured value saturated. A magnified region in Figure 3d and the θ/V plot (Figure 3f) show this more clearly. Green arrows mark the receding experiments and there is an RCA "plateau" at 33°, after which the CA does not decrease anymore. In the baseline length vs time plot (Figure 3c), there was a clear point where the baseline started to recede abruptly (marked with a red arrow) and it corresponded exactly with the onset of the RCA plateau. A close inspection showed that there was always a slight decrease in the baseline length before the turning point (i.e., just before the red arrow in Figure 3c). This pseudo-movement of the contact line is explained qualitatively with the following experiment: a 120 μL drop was allowed to freely evaporate in ambient conditions (without needle in the drop) and the time-dependent behavior was measured (see Supporting Information Figure S3). We observed that at first the baseline length *increased* very slightly, and when the RCA was reached, it started to recede. During the initial evaporation phase (before receding), there are two competing phenomena: the drop size decreases due to evaporation and thus acts to decrease the

dx.doi.org/10.1021/la400009m | *Langmuir* 2013, 29, 3858–3863

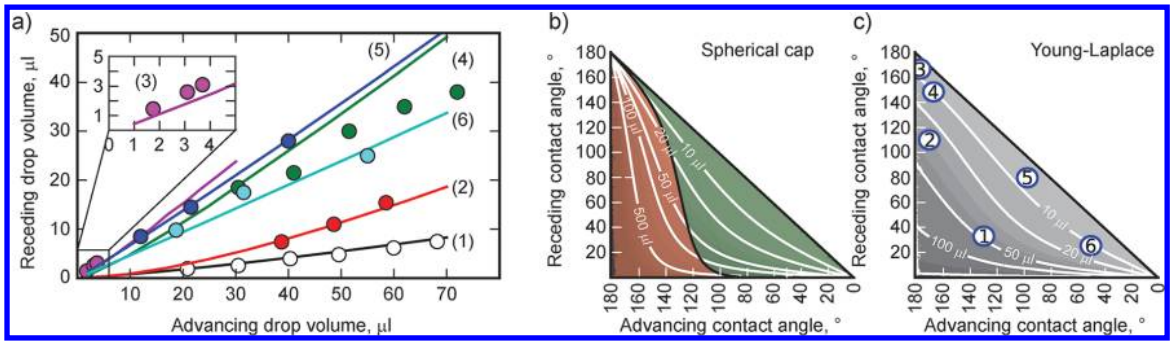

Figure 4. Evaluation of the measured contact angle data to the Young−Laplace model and both of the theoretical models visualized. (a) The solid lines represent results from solving the Young−Laplace equation. The data (symbols) correspond well with the Young−Laplace equation. Note that there are no fitting variables, but the curves come from the ACA and the RCA alone. (b) Advancing drop volume needed to reach the RCA at 5 μL calculated using the spherical cap approximation. The colored regions show how well the spherical cap approximation follows the Young−Laplace solution: the green regions deviate less than 50%, while the red regions deviate more. The spherical cap model performs well for surfaces with an ACA lower than ca. 120° or when there is small hysteresis. (c) Same as b, but solved by integrating the Young−Laplace equation. The numbered circles show where each of the surfaces are located on the graph.

baseline length; and due to vibrations, the CA relaxes toward the MSCA, which increases the baseline length. When liquid was pumped out of the drop, it effectively made the former process faster, which could explain why the contact line initially receded slightly during needle-in-the-drop measurements, yet advanced during evaporation experiments. In conclusion, the initial slow receding movement of the contact line, before the RCA plateau was reached, was caused by the liquid pumping action and could be considered an artifact.

Figure 3e shows photographs from an RCA measurement. First, the drop volume was 10 μL and the CA was at the ACA (129°). When the drop volume was reduced to 5 μL, the CA reached the value of 96°, which was not the real RCA, as the contact line was not yet properly receding. Next, the drop volume was increased to 69 μL and the CA was at the ACA. Now, decreasing the drop volume to 10 μL gave a completely different result of 33°, which was the real RCA value. Figure 3g shows the size-dependent behavior schematically on a θ/V plot.

"Stick and slip" behavior (see Supporting Information Figure S6) during the RCA measurements was detrimental, as the time when the baseline was receding between the jumps was so short that the CA could not be measured. Often, sticking also occurred only on one side of the drop, which skewed the drop shape so much that an axisymmetric fit was impossible. For this reason, it is important that the RCA is reached at a high enough volume. We determined that 5 μL is often an adequate lower limit for the RCA plateau, but if the "stick and slip" behavior is pronounced, an even higher volume might be necessary. Furthermore, the standard deviation of an RCA measurement could be narrowed down by using a longer plateau region. The RCA for surface (1) was determined as 32.6° ± 1.6° with an advancing drop volume of 30 μL and 32.5° ± 0.6° for 70 μL (error is the standard deviation from a single experiment).

To calculate the drop size needed for a reliable RCA measurement, we first consider a simple model for small drops where the effect of gravity is neglected (i.e., Bond number, $\rho g L^2/\gamma \ll 1$). In this case, the drop is represented by a spherical cap. For a spherical cap drop with a contact angle of θ (here, θ can be any CA), the volume is given by

$$V = \frac{\pi}{3}R^3(x^3 - 3x + 2) \qquad \text{where} \qquad x = \cos\theta \tag{1}$$

Now let us assume that the drop has reached its ACA with volume V_a and diameter of the circle contacting the substrate is L. Next the volume of the drop is reduced. The drop contact area diameter does not change until the RCA is reached. At that point, drop volume is V_r. Using $L = 2R \sin\theta$, eq 1 can be reformulated to

$$L^3 = \frac{24V_a}{\pi}({x_a}^3 - 3x_a + 2)^{-1}(1 - {x_a}^2)^{3/2} = \frac{24V_r}{\pi}({x_r}^3 - 3x_r + 2)^{-1}(1 - {x_r}^2)^{3/2} \tag{2}$$

where the subscripts a and r refer to either advancing or receding drops. Equating the advancing and the receding drop contact diameters leads to a linear relation between the two:

$$V_r = f(x_a, x_r)V_a \qquad \text{where} \tag{3}$$

$$f(x_a, x_r) = \frac{(x_r - 1)^2(x_r + 2)(1 - {x_r}^2)^{-3/2}}{(x_a - 1)^2(x_a + 2)(1 - {x_a}^2)^{-3/2}} \tag{4}$$

If both the ACA and the RCA are known, eq 3 can be used to calculate what the minimum initial advancing drop size should be to reach the RCA plateau at a certain volume. For example, if we assume that the RCA should be reached at V_r = 5 μL, we get ca. V_a = 85 μL for the advancing drop volume for surface (1), and V_a = 800 μL for surface (2). The spherical cap model exaggerates the volume needed for the advancing drop for high contact angles, yet shows the principle qualitatively and can still be used when the ACA is lower than ca. 120° or the hysteresis is low (see Figure 4). Similarly calculated advancing drop volumes for all the ACA/RCA combinations can be found in Figure 4b. To achieve more accurate results, drop volumes were calculated by solving the Young−Laplace equation in the axisymmetric case using discretization along the drop perimeter[20] and numerical integration (details are given in the Supporting Information). As seen from Figure 4a, the results from the Young−Laplace model matched well with the experimental data. Note that the curves were not fitted, but the parameters (ACA, RCA) were given by the CA measurements.

To make predictions about the minimum volume of the ACA drop, we assumed that the RCA plateau should be reached at 5 μL. Thus, the ACA volume was calculated for all (θ_a, θ_r) pairs using both spherical cap and Young−Laplace models. The results are plotted in Figure 4b,c, which, for example, shows that, if expected hysteresis is less than 10°, an advancing drop volume of 10−15 μL should be adequate in most cases, yet if

dx.doi.org/10.1021/la400009m | Langmuir 2013, 29, 3858−3863

expected hysteresis is 30°, the advancing drop volume should be at least 20 μL. Figure 4b also shows how the spherical cap model compares to the Young−Laplace model. For small hysteresis, the spherical cap model can be used, yet it fails for both high ACAs and low RCAs. Black line represents the limit where the spherical cap model deviates from the Young−Laplace model by more than 50%.

To test the model we used six different surfaces, which spread over the entire contact angle range. Figure 4a shows how the model corresponds with each surface. Surfaces (1), (2), and (5) follow the Young−Laplace calculations well. However, with surfaces (4) and (6), there is a decreasing trend at large volumes. The model seems to function best when there is a substantial amount of hysteresis, yet it is irrespective of the actual contact angles. Surface (3) was a special case, as it had extremely low hysteresis and is strictly the only one we would qualify as superhydrophobic. To gain an accurate measurement, we could not use large drop volumes, as the initial CA decrease phase could not be found, but the contact line started to recede immediately. This artifact was mostly due to the poor spatial resolution of the camera at that magnification. By using smaller drops with volumes of less than 5 μL, both the ACA and the RCA of surface (3) could be measured, when the magnification of the camera was adjusted to a higher value. The measured data followed the theoretical curve (the inset in Figure 4a) well, which confirmed that the model performs well also for superhydrophobic surfaces and with smaller drop volumes. However, we would advise using larger drop volumes whenever possible to minimize the problems related to "stick and slip" or inhomogeneities of the surface. This also reduces the standard deviation of the RCA measurement.

All of the measured surfaces were exclusively in either the Cassie-Baxter or Wenzel wetting state and did not show transitions during the experiments. However, there are numerous examples where a surface exhibits both Cassie-Baxter and Wenzel behavior depending on, for example, pressure exerted on the surface,[25,24] drop size,[26,27] or impact velocity.[28−30] Therefore, we simulated a contact angle measurement where the drop started in Cassie-Baxter state, yet transitioned to the Wenzel state at a critical pressure (see the Supporting Information). The results were exactly the same as with only the Cassie-Baxter or Wenzel state, but the surface switched between the two. Repeated cycles of measurement thus gave first the Cassie-Baxter values and then the Wenzel values. The model yields accurate results also for these surfaces, yet care has to be taken to identify whether such a transition occurs.

In conclusion, we have shown that the RCA can be reliably measured from different surfaces with varying contact angles and hysteresis using the needle-in-sessile-drop method: Deposit a small drop on the surface and leave the needle inside the drop. Continuously record the CA using a Young−Laplace based fit. Increase the drop volume. Use eq 3 or Figure 4c as a guideline to determine the final volume. Decrease the drop volume slowly until ca. 2 μL. Find the "plateau" regions and determine the ACA and the RCA together with standard deviation.

The initial size of the drop is the key to a successful RCA measurement. This is clearly demonstrated for a surface with both a high ACA and large hysteresis, yet surfaces with low hysteresis exhibit similar behavior. For the RCA measurements, the contact line should recede long enough to reach a narrow standard deviation and we consider 5 μL as a reasonable lower limit. Furthermore, eq 3 and Figure 4c can be used as guidelines when planning CA measurements, when there is a reasonable guess for the hysteresis. From the figure, one can note that in many cases it is not sufficient to use drop sizes less than 10 μL, yet sometimes even values up to 50 μL are needed. The method is not restricted to needle-in-the-drop experiments and applies also to freely evaporating drops. It is even possible to measure surfaces, which exhibit a wetting transition during the experiment.

■ ASSOCIATED CONTENT

Supporting Information

Detailed experimental procedures along with contact angle measurement data for all surfaces. Scanning electron micrographs of the surfaces. Solving the Young−Laplace equation. Numerical integration algorithm for solving the Young−Laplace equation. Explanation of the stick and slip behavior. Details of the simulated contact angle measurements and an example of how to identify a wetting transition during an experiment. This material is available free of charge via the Internet at http://pubs.acs.org.

■ AUTHOR INFORMATION

Corresponding Author

*E-mail: robin.ras@aalto.fi.

Notes

The authors declare no competing financial interest.

■ ACKNOWLEDGMENTS

Funding from the Academy of Finland is acknowledged. This work made use of Aalto University Nanomicroscopy Center (Aalto-NMC) facilities. Jaana Vapaavuori is thanked for checking the details of the theory part. A special thanks is given to Jason McKee for proofreading the text.

■ REFERENCES

(1) Neinhuis, C.; Barthlott, W. Characterization and Distribution of Water-repellent, Self-cleaning Plant Surfaces. *Ann. Bot.* **1997**, *79*, 667−677.

(2) Barthlott, W.; Neinhuis, C. Purity of the Sacred Lotus, or Escape from Contamination in Biological Surfaces. *Planta* **1997**, *202*, 1−8.

(3) Shirtcliffe, N. J.; McHale, G.; Atherton, S.; Newton, M. I. An Introduction to Superhydrophobicity. *Adv. Colloid Interface Sci.* **2010**, *161*, 124−138.

(4) Wenzel, R. N. Resistance of Solid Surfaces to Wetting by Water. *Ind. Eng. Chem.* **1936**, *28*, 988−994.

(5) Cassie, A. B. D.; Baxter, S. Wettability of Porous Surfaces. *Trans. Faraday Soc.* **1944**, 546−551.

(6) We found the oldest occurrences of "superhydrophobic" from two patents (refs 7 and 8), where the word is used like an already established term.

(7) Reick, F. G. Substrate Coated with Super-Hydrophobic Layers. U.S. Patent 3,931,428, Jan 6, 1976.

(8) Reick, F. G. Toys and Games Using Super-Hydrophobic Surfaces. U.S. Patent 4,199,142, Apr 22, 1980.

(9) Drelich, J.; Chibowski, E.; Meng, D. D.; Terpilowski, K. Hydrophilic and Superhydrophilic Surfaces and Materials. *Soft Matter* **2011**, *7*, 9804−9828.

(10) Macdougall, G.; Ockrent, C. Surface Energy Relations in Liquid/Solid Systems. I. The Adhesion of Liquids to Solids and a New Method of Determining the Surface Tension of Liquids. *Proc. R. Soc. London, Ser. A* **1942**, *180*, 151−173.

(11) Krasovitski, B.; Marmur, A. Drops Down the Hill: Theoretical Study of Limiting Contact Angles and the Hysteresis Range on a Tilted Plate. *Langmuir* **2005**, *21*, 3881−3885.

(12) Blake, T. D. The Physics of Moving Wetting Lines. *J. Colloid Interface Sci.* **2006**, *299*, 1−13.
(13) Marmur, A. A Guide to the Equilibrium Contact Angles Maze. In *Contact Angle, Wettability and Adhesion*, Mittal, K. L., Ed.; VSP: Leiden, 2009; Vol. *6*, Chapter 1.1.
(14) Andrieu, C.; Sykes, C.; Brochard, F. Average Spreading Parameter on Heterogeneous Surfaces. *Langmuir* **1994**, *10*, 2077−2080.
(15) Decker, E. L.; Garoff, S. Using Vibrational Noise To Probe Energy Barriers Producing Contact Angle Hysteresis. *Langmuir* **1996**, *12*, 2100−2110.
(16) Montes Ruiz-Cabello, F. J.; Rodríguez-Valverde, M. A.; Cabrerizo-Vílchez, M. A New Method for Evaluating the Most Stable Contact Angle Using Tilting Plate Experiments. *Soft Matter* **2011**, *7*, 10457−10461.
(17) Zimmermann, J.-H. Silicone Nanofilaments as Functional Coatings: Properties, Applications and Modifications. Ph.D. Thesis, University of Zürich, 2008.
(18) Zhang, X.; Shi, F.; Niu, J.; Jiang, Y.; Wang, Z. Superhydrophobic Surfaces: From Structural Control to Functional Application. *J. Mater. Chem.* **2008**, *18*, 621−633.
(19) Srinivasan, S.; McKinley, G. H.; Cohen, R. E. Assessing the Accuracy of Contact Angle Measurements for Sessile Drops on Liquid-Repellent Surfaces. *Langmuir* **2011**, *27*, 13582−13589.
(20) Hoorfar, M.; Neumann, A. W. Axisymmetric Drop Shape Analysis (ADSA). In *Applied Surface Thermodynamics*, 2nd ed.; Neumann, A. W., David, R., Zuo, Y., Eds.; CRC Press: Boca Raton, 2010; Chapter 3, pp 107−174.
(21) Artus, G.; Jung, S.; Zimmermann, J.; Gautschi, H.-P.; Marquardt, K.; Seeger, S. Silicone Nanofilaments and Their Application as Superhydrophobic Coatings. *Adv. Mater.* **2006**, *18*, 2758−2762.
(22) Gao, L.; McCarthy, T. J. A Perfectly Hydrophobic Surface (θ_A/θ_R = 180°/180°). *J. Am. Chem. Soc.* **2006**, *128*, 9052−9053.
(23) Rollings, D. E.; Tsoi, S.; Sit, J. C.; Veinot, J. G. C. Formation and Aqueous Surface Wettability of Polysiloxane Nanofibers Prepared via Surface Initiated, Vapor-Phase Polymerization of Organotrichlorosilanes. *Langmuir* **2007**, *23*, 5275−5278.
(24) Verho, T.; Korhonen, J. T.; Sainiemi, L.; Jokinen, V.; Bower, C.; Franze, K.; Franssila, S.; Andrew, P.; Ikkala, O.; Ras, R. H. A. Reversible Switching Between Superhydrophobic States on a Hierarchically Structured Surface. *Proc. Natl. Acad. Sci. USA* **2012**, *109*, 10210−10213.
(25) Lafuma, A.; Quéré, D. Superhydrophobic States. *Nat. Mater.* **2003**, *2*, 457−60.
(26) Bico, J.; Marzolin, C.; Quéré, D. Pearl Drops. *Europhys. Lett.* **1999**, *47*, 220−226.
(27) Yoshimitsu, Z.; Nakajima, A.; Watanabe, T.; Hashimoto, K. Effects of Surface Structure on the Hydrophobicity and Sliding Behavior of Water Droplets. *Langmuir* **2002**, *18*, 5818−5822.
(28) He, B.; Patankar, N. A.; Lee, J. Multiple Equilibrium Droplet Shapes and Design Criterion for Rough Hydrophobic Surfaces. *Langmuir* **2003**, *19*, 4999−5003.
(29) Bartolo, D.; Bouamrirene, F.; Verneuil, É.; Buguin, A.; Silberzan, P.; Moulinet, S. Bouncing or Sticky Droplets: Impalement Transitions on Superhydrophobic Micropatterned Surfaces. *Europhys. Lett.* **2006**, *74*, 299−305.
(30) Hipp, B.; Kunert, I.; Dürr, M. Systematic Control of Hydrophobic and Superhydrophobic Properties Using Double−Rough Structures Based on Mixtures of Metal Oxide Nanoparticles. *Langmuir* **2010**, *26*, 6557−60.